Robust kagome electronic structure in the topological quantum magnets $X\mathrm{Mn_6Sn_6}$ (X = Dy, Tb, Gd, Y)

X. Gu,[1,*] C. Chen,[2,3,4,*] W. S. Wei,[5] L. L. Gao,[2] J. Y. Liu,[6] X. Du,[1] D. Pei,[6] J. S. Zhou,[1] R. Z. Xu,[1] Z. X. Yin,[1] W. X. Zhao,[1] Y. D. Li,[1] C. Jozwiak,[4] A. Bostwick,[4] E. Rotenberg,[4] D. Backes,[7] L. S. I. Veiga,[7] S. Dhesi,[7] T. Hesjedal,[7] G. van der Laan,[7] H. F. Du,[5] W. J. Jiang,[1,8] Y. P. Qi,[2,3,9] G. Li,[2,3] W. J. Shi,[10,11] Z. K. Liu,[2,3,†] Y. L. Chen,[1,2,3,6,‡] and L. X. Yang[1,8,§]

[1]*State Key Laboratory of Low Dimensional Quantum Physics, Department of Physics, Tsinghua University, Beijing 100084, China*

[2]*School of Physical Science and Technology, ShanghaiTech University and CAS-Shanghai Science Research Center, Shanghai 201210, China*

[3]*ShanghaiTech Laboratory for Topological Physics, Shanghai 200031, China*

[4]*Advanced Light Source, Lawrence Berkeley National Laboratory, Berkeley, California 94720, USA*

[5]*Anhui Province Key Laboratory of Condensed Matter Physics at Extreme Conditions, High Magnetic Field Laboratory of the Chinese Academy of Sciences, Hefei 230026, China*

[6]*Department of Physics, Clarendon Laboratory, University of Oxford, Parks Road, Oxford OX1 3PU, United Kingdom*

[7]*Diamond Light Source, Harwell Science and Innovation Campus, Didcot OX11 0DE, United Kingdom*

[8]*Frontier Science Center for Quantum Information, Beijing 100084, China*

[9]*Shanghai Key Laboratory of High-resolution Electron Microscopy, Shanghai Tech University, Shanghai 201210, China*

[10]*Center for Transformative Science, ShanghaiTech University, Shanghai 201210, China*

[11]*Shanghai High Repetition Rate XFEL and Extreme Light Facility (SHINE), ShanghaiTech University, Shanghai 201210, China*

(Received 9 October 2021; revised 19 December 2021; accepted 18 March 2022; published 5 April 2022)

Crystal geometry can greatly influence the emergent properties of quantum materials. As an example, the kagome lattice is an ideal platform to study the rich interplay between topology, magnetism, and electronic correlation. In this work, combining high-resolution angle-resolved photoemission spectroscopy and *ab initio* calculation, we systematically investigate the electronic structure of $X\mathrm{Mn_6Sn_6}$ (X = Dy, Tb, Gd, Y) family compounds. We observe the Dirac fermion and the flat band arising from the magnetic kagome lattice of Mn atoms. Interestingly, the flat band locates in the same energy region in all compounds studied, regardless of their different magnetic ground states and $4f$ electronic configurations. These observations suggest a robust Mn magnetic kagome lattice across the $X\mathrm{Mn_6Sn_6}$ family, thus providing an ideal platform for the search for, and investigation of, new emergent phenomena in magnetic topological materials.

DOI: 10.1103/PhysRevB.105.155108

Kagome lattice, a two-dimensional network of corner-sharing triangles, exhibits many novel emergent properties such as spin liquids in frustrated magnets [1–3], competition between superconductivity and charge-density waves [4,5], and interplay between magnetism, topology, and electron correlation [6–12]. In particular, the destructive interference of Bloch electrons gives rise to flat bands that can be described by Chern numbers, mimicking the Landau levels without an external magnetic field [13]. When the flat bands are partially filled, a fractional quantum Hall state can be naturally realized [14,15]. In addition, as the kagome lattice is structurally a sibling of the honeycomb lattice, Dirac fermions exist at the corners of the Brillouin zone [Fig. 1(a)], similar to the physics in graphene [16]. If the time-reversal symmetry is broken (e.g., by ferromagnetic ordering), the band degeneracy of the Dirac cones will be lifted and a Chern gap will be induced as a result of the spin-orbit coupling [Fig. 1(b)], leading to the quantum anomalous Hall effect [17–19].

While the kagome model considers s-electrons and nearest-neighbor interaction, the situation is much more complex in real magnetic materials. On the one hand, many magnetic kagome materials involve $3d$-electrons with strong electron correlation; on the other hand, the kagome lattices in real materials usually consist of more than one type of atom and may not be the ideal form due to their three-dimensional (3D) or quasi-two-dimensional (2D) crystal structure, making the realization of proposed topological electronic structures challenging. Although some intriguing phenomena owing to the Berry curvature of their topological electronic structures, such as the large anomalous Hall effect, have been observed in several kagome magnets [7,10,20–22], direct visualization of the massive Dirac fermions is still limited. Moreover, the characteristic flat bands near the Fermi level (E_F) are mainly observed in paramagnetic kagome materials so far, while in ferromagnetic kagome materials, the flat bands usually reside well below (>200 meV) E_F [9,12,23–26], making the interplay between the magnetism and kagome-related physics less straightforward. Recently, it was proposed that there exists an ideal kagome lattice with quantum-limit Chern topological

*These authors contributed equally to this work.
†liuzhk@shanghaitech.edu.cn
‡yulin.chen@physics.ox.ac.uk
§lxyang@tsinghua.edu.cn

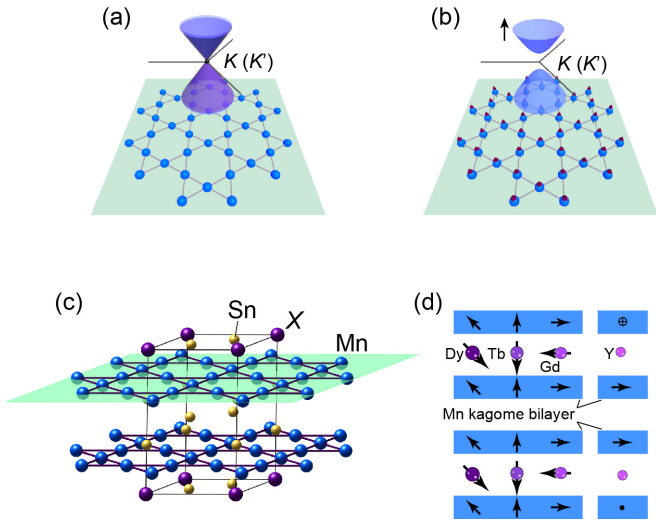

FIG. 1. (a) Nonmagnetic kagome lattice with a gapless Dirac cone at the K point of the Brillouin zone (BZ). (b) Ferromagnetic kagome lattice with a gapped Dirac cone at K. (c) Crystal structure of $X\mathrm{Mn_6Sn_6}$ (X = Dy, Tb, Gd, Y). The green plane highlights the kagome layer of Mn atoms. (d) Schematic of the magnetism of $X\mathrm{Mn_6Sn_6}$ at low temperatures. The kagome layers of Mn atoms show different ferromagnetism for rare-earth materials, while the Mn layers in $\mathrm{YMn_6Sn_6}$ show a helical antiferromagnetism. The magnetization of the X atoms changes in different compounds.

magnetism in $X\mathrm{Mn_6Sn_6}$ (X = Dy, Tb, Gd, Y) family compounds, where the kagome layers are constructed solely by the Mn atoms [7]. The existence of massive Dirac fermions at the K point has been indicated by the observation of Landau quantization and a Landau fan diagram in $\mathrm{TbMn_6Sn_6}$ [7], and the flat band together with the Dirac cone has been directly observed in $\mathrm{YMn_6Sn_6}$ and $\mathrm{GdMn_6Sn_6}$ [26,27]. Nevertheless, the systematic evolution of the electronic structure of the $X\mathrm{Mn_6Sn_6}$ family and the influence of the magnetism with variable X atoms still await further experimental exploration.

In this work, we systematically investigate the electronic structures of $X\mathrm{Mn_6Sn_6}$ (X = Dy, Tb, Gd, Y) family compounds combining the use of high-resolution angle-resolved photoemission spectroscopy (ARPES) and *ab initio* calculation (methods in the Supplemental Material [28]). Our experiment reveals the multiband nature of the electronic structure near E_F derived from Mn 3d orbitals that shows clear k_z dispersion, suggesting the important role of interkagome-layer coupling. We also observe characteristic electronic structures of the Mn kagome lattice: the Dirac fermion near E_F at the K point and the flat bands, consistent with our *ab initio* calculations. Remarkably, the observed kagome band structures in different compounds are almost identical, suggesting a minor influence of the magnetic ordering and f-electron configuration on the electronic structure of the Mn kagome layer. These observations not only provide insights into the interplay between magnetism, crystal geometry, correlation, and topology, but also shed light on the future study of novel emergent phenomena in magnetic topological materials.

$X\mathrm{Mn_6Sn_6}$ crystallizes into a hexagonal structure with the space group of $P6/mmm$. Each unit cell contains an X-Sn layer and two Mn-Sn layers separated by a honeycomb layer of Sn atoms. Within each Mn-Sn layer, the Mn atoms form a 2D kagome lattice [Fig. 1(c)], providing an ideal platform for the study of kagome-related emergent physics. At room temperature, the magnetic moments of the Mn atoms align ferromagnetically within each kagome layer, while the X atoms engineer the overall magnetic ground state of the system [29–31] [Fig. 1(d)]. In the compounds with X = Dy, Tb, and Gd, adjacent Mn kagome bilayers couple ferromagnetically across the magnetic X-Sn layer, inducing ferrimagnetism with different magnetic anisotropies in the system [29,30], as shown in Fig. 1(d). In $\mathrm{YMn_6Sn_6}$, by contrast, the Y atom exhibits no magnetization, thus the adjacent ferromagnetic kagome bilayers couple antiferromagnetically across the nonmagnetic Y-Sn layer, inducing complex helical antiferromagnetism below 300 K [32]. Details of the magnetism of $X\mathrm{Mn_6Sn_6}$ compounds can be found in the Supplemental Material [28].

Figure 2 shows the electronic structure of a representative compound, $\mathrm{DyMn_6Sn_6}$, measured at 12 K (no change in the magnetism of $X\mathrm{Mn_6Sn_6}$ compounds is observed below 100 K) (Supplemental Material, Fig. S1 [28]). We observe clear k_z variation of the electronic states near E_F (Supplemental Material, Fig. S3 [28]), as shown in the Fermi surface (FS) in the k_z–$k_{||}$ plane in Fig. 2(b), indicating the strong interlayer coupling (the inner potential used in the estimation of k_z values is 10 eV). Figure 2(c) shows the evolution of the constant energy contours with the binding energy at the ΓKM plane (measured with 138-eV photon energy). The FS consists of a warped electron pocket around the Γ point and triangle features near the K point, which gradually evolve into a dot and corner-connected triangles, respectively, with increasing binding energy. Figure 2(d) presents the 3D plot of the band structure showing sharp dispersions crossing E_F along both the ΓM and ΓK directions with clear anisotropy. Figures 2(e) and 2(f) show the band dispersions along high-symmetry directions measured with different photon polarizations. In the linear-horizontal (LH) channel, we observe two bands (the inner α band and the outer β band) crossing E_F around Γ. The α band crosses E_F along both ΓK and ΓM, forming the warped FS around Γ, while the β band forms a Dirac cone near E_F at the K point, which is the characteristic feature of the kagome lattice. In the linear-vertical (LV) channel, except for the β band observed in LH channel, two other bands crossing E_F (γ and δ) are evidenced. Interestingly, the δ band has an electron-like dispersion along KM, while all the bands show hole-like dispersion along ΓM. Therefore, the δ band forms a saddle point near the M point (Supplemental Material, Fig. S5 [28]), which is another characteristic feature anticipated in the kagome lattice. In Fig. 2(g), the calculated band structure, after being renormalized by a factor of 2.75 and shifted by 35 meV, is superposed with experimentally extracted band dispersions around the Dirac point at K. The observed band structure near the Dirac point can be well captured by the calculation with spin-orbit coupling included, which predicts a nearly gapless Dirac cone (energy gap < 5 meV) near E_F. Noticeably, our calculation suggests another Dirac cone with a large energy gap ($\sim$30 meV) at 100 meV above E_F, in good agreement with the simulation of the Landau fan data [7].

To investigate the influence of the X atoms on the electronic structure further, we compare the electronic structures

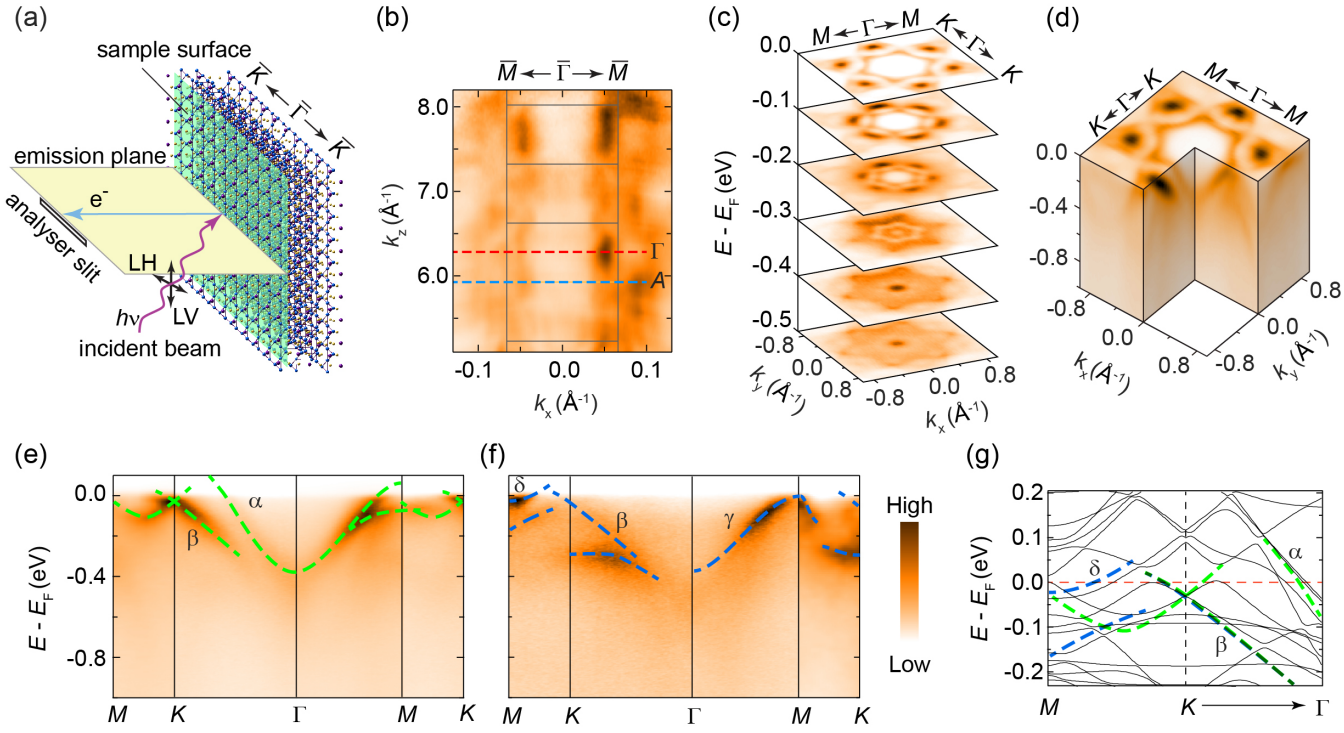

FIG. 2. (a) ARPES geometry used in our experiments. (b) FS of $DyMn_6Sn_6$ in the k_z-k_x plane measured with a photon energy-dependent ARPES experiment. (c) Evolution of the constant energy contours with binding energy measured with 138-eV photon energy. (d) 3D plot of the electronic structure on the k_x-k_y plane. (e), (f) Band structure along high-symmetry directions measured with (e) linear-horizontally (LH) and (f) linear-vertically (LV) polarized photons at 138 eV. The green and blue curves are a guide to the eyes for the measured dispersion. Note that the Fermi momenta of the α and γ bands are different. (g) Comparison of the measured and calculated band structure along high-symmetry directions. The black curves are the calculated band structures after being renormalized by a factor of about 2.75 and shifted by 35 meV. Data were collected at 12 K.

of different XMn_6Sn_6 compounds, as illustrated in Figs. 3(a)–3(d). The FS structure in general does not change with variation of the X element, even for the nonmagnetic Y atoms, suggesting the weak influence of the X element and the ro-

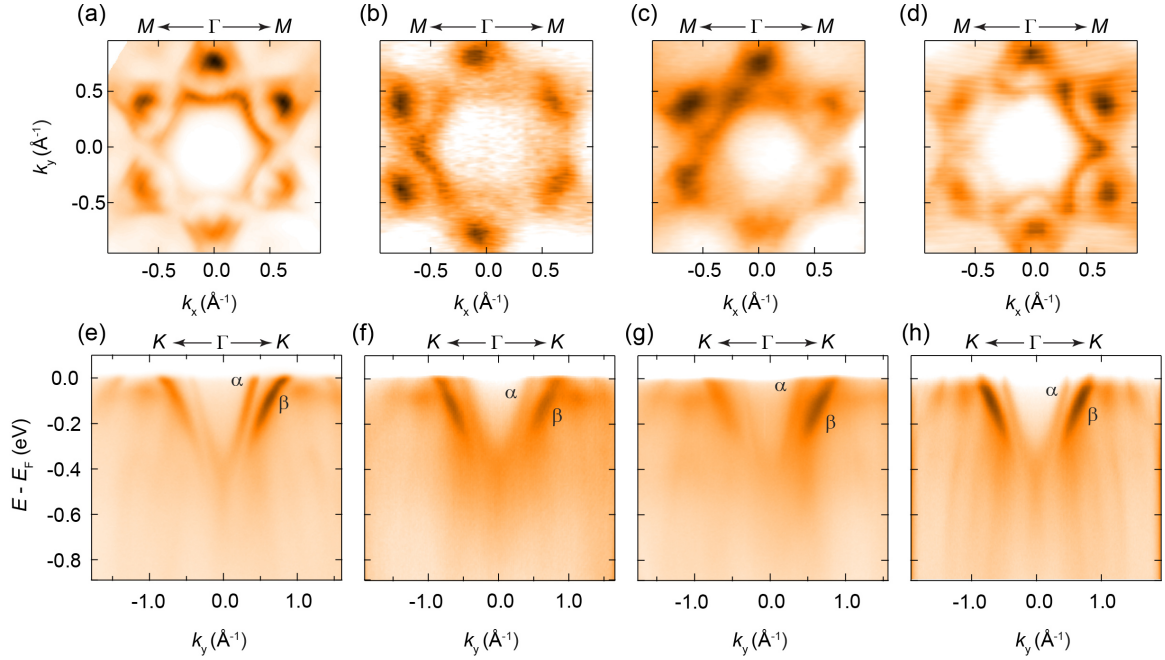

FIG. 3. (a)–(d) FS of (a) $DyMn_6Sn_6$, (b) $TbMn_6Sn_6$, (c) $GdMn_6Sn_6$, and (d) YMn_6Sn_6. (e)–(h) Band dispersion along ΓKM in different compounds. Data were collected using LH polarized photons at 138 eV at 12 K.

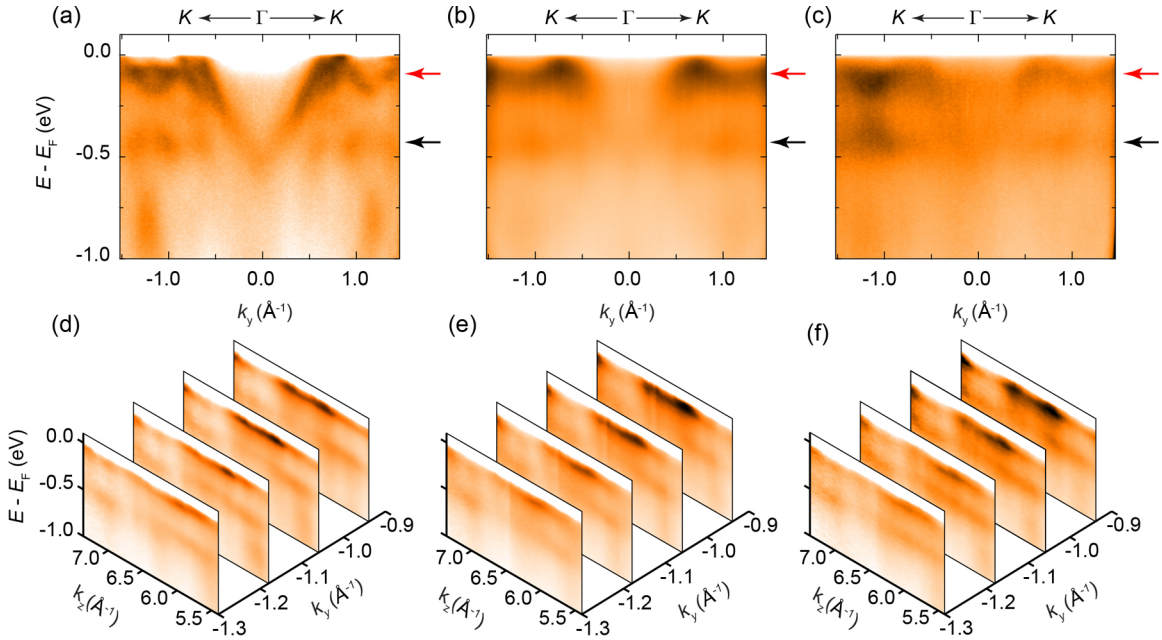

FIG. 4. (a)–(c) Band dispersion of (a) $DyMn_6Sn_6$, (b) $TbMn_6Sn_6$, and (c) $GdMn_6Sn_6$ along ΓKM. (d)–(f) Band dispersions of XMn_6Sn_6 along k_z at different k_y. (a)–(c) are the summation of the data measured with LH and LV polarized photons at 112 eV. Data in (d)–(f) were collected using LH polarized photons. All data were collected at 12 K.

bustness of the Mn kagome lattice. Consistently, similar band dispersions along ΓKM are observed in all the four compounds studied [Figs. 3(e)–3(h)], with only a small variation of the Fermi momenta of the α band, possibly induced by a slight change of the doping level with different X atoms.

Our *ab initio* calculation indicates the existence of flat bands around 0.4 eV below E_F that originate from Mn d_{z^2} orbitals {Fig. 2(g) and Supplemental Material, Fig. S5 [28]}. To search for these flat bands, we conducted photon energy-dependent ARPES measurements over a large energy range (60 to 200 eV), with the results demonstrated in Fig. 4. Due to the orbital characters of the flat bands, they are better visualized using LV photons (Supplemental Material, Fig. S8 [28]). Figure 4(a) shows the ARPES spectrum along the $\Gamma K M$ direction measured on $DyMn_6Sn_6$ using 112-eV photons, and as expected, the flat band is clearly observed at 0.42 eV below E_F. Figures 4(b) and 4(c) illustrate the result of the same measurements on $TbMn_6Sn_6$ and $GdMn_6Sn_6$, and similar flat bands are ubiquitously observed. The flat band can also be clearly seen in the measurements along the k_z direction at different k_y values [Figs. 4(d)–4(f)], with minor differences among different compounds. In addition, a second flat band is observed around −100 meV for all compounds, as indicated by the red arrows in Figs. 4(a)–4(c), which was likewise observed in the extended Brillouin zone in YMn_6Sn_6 [26].

Despite the change of the X atoms and the magnetism configuration of the system, the kagome band structure of XMn_6Sn_6 remains almost the same (Fig. 4, also see Supplemental Material, Figs. S4 and S7 [28]), suggesting a robust and ideal platform to investigate and engineer the kagome-related physics. Nevertheless, we notice that the flat bands are not observed over the whole Brillouin zone and show weak dispersion, with a band width of about 50 meV (Fig. 4), which may result from the strong interkagome-layer coupling. Quantum-limit kagome physics is expected in the atomically thin Mn-Sn layer if it can be isolated from XMn_6Sn_6 or synthesized by molecular beam epitaxy. Moreover, if the Fermi level can be tuned into the large gap of the Dirac cone at about 100 meV above E_F [Fig. 2(g)], interesting quantum effects, such as quantum anomalous Hall effect, may be realized.

In addition, the XMn_6Sn_6 compounds provide an ideal platform to study the interplay between correlation and topology [27]. The correlation effect usually plays an important role in the $3d$ electronic systems, manifested here in different ways in the XMn_6Sn_6 system. First, a moderate band renormalization factor of about 2.75 has to be used to compare the calculated and observed band structure. Second, highly dispersive bands with a band width larger than 1 eV are observed [Figs. 3(e)–3(h)], in drastic contrast to the calculation but reminiscent of the waterfall dispersions in cuprates and iridates [33–37], indicating the impact of electronic correlation on the electronic structure of XMn_6Sn_6. Third, the bands below 0.5 eV are strongly blurred and/or disappear in our experiment, suggesting that the electronic states are incoherent at high binding energies, which is commonly observed in correlated materials [38–40]. Finally, the $4f$-electrons of the rare-earth elements Dy, Tb, and Gd seem not to interact strongly with Mn $3d$-electrons, and their influence on the flat bands of the kagome layer is negligible. Nevertheless, the waterfall dispersion is suppressed and blurred in rare-earth compounds compared to that in YMn_6Sn_6 (Fig. 3), suggesting that the $4f$-electrons do contribute to the correlation effect in XMn_6Sn_6. The complex correlation effect requires further experimental and theoretical investigation to understand its interplay with the magnetism and topology in these kagome materials.

In conclusion, we have systematically studied the electronic structure of magnetic kagome materials $X\mathrm{Mn_6Sn_6}$ and observed the Dirac cone, the saddle point, and flat bands that are characteristic features of the electronic structure of a kagome lattice. The observed electronic structure, particularly the flat bands, is robust against the change in the magnetic moment and $4f$ electronic configuration related to the X atoms. Our results not only provide important insights into the electronic structure of an ideal family of magnetic kagome materials, but also suggest an interesting platform to investigate novel topological kagome physics and its interplay with magnetism and correlation effects. We further propose that rich and intriguing phenomena are expected in the atomically thin films of the Mn kagome layer.

ACKNOWLEDGMENTS

This work was supported by the National Natural Science Foundation of China (Grants No. 11774190, No. 11674229, and No. 11634009), the National Key R&D Program of China (Grants No. 2017YFA0304600 and No. 2017YFA0305400), and an EPSRC Platform Grant (Grant No. EP/M020517/1). W. J. S. acknowledges support from the Shanghai-XFEL Beamline Project (31011505505885920161A2101001). The calculations were carried out at the Scientific Data Analysis Platform of Center for Transformative Science and the HPC Platform of ShanghaiTech University Library and Information Services. This research used resources of the Advanced Light Source, a US DOE Office of Science User Facility under Contract No. DE-AC02-05CH11231. Diamond Light Source is acknowledged for beamtime at beamline I06 under proposal No. MM27482.

[1] L. Balents, Nature (London) **464**, 199 (2010).
[2] T.- H. Han, J. S. Helton, S. Chu, D. G. Nocera, J. A. Rodriguez-Rivera, C. Broholm, and Y. S. Lee, Nature (London) **492**, 406 (2012).
[3] M. Fu, T. Imai, T.- H. Han, and Y. S. Lee, Science **350**, 655 (2015).
[4] B. R. Ortiz, L. C. Gomes, J. R. Morey, M. Winiarski, M. Bordelon, J. S. Mangum, I. W. H. Oswald, J. A. Rodriguez-Rivera, J. R. Neilson, S. D. Wilson, E. Ertekin, T. M. McQueen, and E. S. Toberer, Phys. Rev. Materials **3**, 094407 (2019).
[5] F. H. Yu, D. H. Ma, W. Z. Zhuo, S. Q. Liu, X. K. Wen, B. Lei, J. J. Ying, and X. H. Chen, Nat. Commun. **12**, 3645 (2021).
[6] B. Bauer, L. Cincio, B. P. Keller, M. Dolfi, G. Vidal, S. Trebst, and A. W. W. Ludwig, Nat. Commun. **5**, 5137 (2014).
[7] J.-X. Yin, W. Ma, T. A. Cochran, X. Xu, S. S. Zhang, H.-J. Tien, N. Shumiya, G. Cheng, K. Jiang, B. Lian *et al.*, Nature (London) **583**, 533 (2020).
[8] I. I. Mazin, H. O. Jeschke, F. Lechermann, H. Lee, M. Fink, R. Thomale, and R. Valentí, Nat. Commun. **5**, 4261 (2014).
[9] M. Kang, L. Ye, S. Fang, J.-S. You, A. Levitan, M. Han, J. I. Facio, C. Jozwiak, A. Bostwick, E. Rotenberg *et al.*, Nat. Mater. **19**, 163 (2020).
[10] L. Ye, M. Kang, J. Liu, F. von Cube, C. R. Wicker, T. Suzuki, C. Jozwiak, A. Bostwick, E. Rotenberg, D. C. Bell *et al.*, Nature (London) **555**, 638 (2018).
[11] J.-X. Yin, S. S. Zhang, H. Li, K. Jiang, G. Chang, B. Zhang, B. Lian, C. Xiang, I. Belopolski, H. Zheng *et al.*, Nature (London) **562**, 91 (2018).
[12] Z. Lin, J.-H. Choi, Q. Zhang, W. Qin, S. Yi, P. Wang, L. Li, Y. Wang, H. Zhang, Z. Sun, L. Wei, S. Zhang, T. Guo, Q. Lu, J. H. Cho, C. Zeng, and Z. Zhang, Phys. Rev. Lett. **121**, 096401 (2018).
[13] Z. Liu, F. Liu, and Y.-S. Wu, Chin. Phys. B **23**, 077308 (2014).
[14] E. Tang, J.-W. Mei, and X.-G. Wen, Phys. Rev. Lett. **106**, 236802 (2011).
[15] T. Neupert, L. Santos, C. Chamon, and C. Mudry, Phys. Rev. Lett. **106**, 236804 (2011).
[16] K. S. Novoselov, A. K. Geim, S. V. Morozov, D. Jiang, M. I. Katsnelson, I. V. Grigorieva, S. V. Dubonos, and A. A. Firsov, Nature (London) **438**, 197 (2005).
[17] G. Xu, B. Lian, and S.-C. Zhang, Phys. Rev. Lett. **115**, 186802 (2015).
[18] K. Ohgushi, S. Murakami, and N. Nagaosa, Phys. Rev. B **62**, R6065 (2000).
[19] W. Zhu, S.-S. Gong, T.-S. Zeng, L. Fu, and D. N. Sheng, Phys. Rev. Lett. **117**, 096402 (2016).
[20] Q. Wang, Y. Xu, R. Lou, Z. Liu, M. Li, Y. Huang, D. Shen, H. Weng, S. Wang, and H. Lei, Nat. Commun. **9**, 3681 (2018).
[21] E. Liu, Y. Sun, N. Kumar, L. Muechler, A. Sun, L. Jiao, S.-Y. Yang, D. Liu, A. Liang, Q. Xu *et al.*, Nat. Phys. **14**, 1125 (2018).
[22] D. Chen, C. Le, C. Fu, H. Lin, W. Schnelle, Y. Sun, and C. Felser, Phys. Rev. B **103**, 144410 (2021).
[23] Z. Liu, M. Li, Q. Wang, G. Wang, C. Wen, K. Jiang, X. Lu, S. Yan, Y. Huang, D. Shen *et al.*, Nat. Commun. **11**, 4002 (2020).
[24] M. Kang, S. Fang, L. Ye, H. C. Po, J. Denlinger, C. Jozwiak, A. Bostwick, E. Rotenberg, E. Kaxiras, J. G. Checkelsky *et al.*, Nat. Commun. **11**, 4004 (2020).
[25] Q. W. T. Y. Yang, Y. H. Wang, M. Song, J. Tang, Z. W. Wang, H. Z. Lv, N. C. Plumb, M. Radovic, G. W. Wang, G. Y. Wang, Z. Sun, R. Yu, M. Shi, Y. M. Xiong, and N. Xu, arXiv:1906.07140.
[26] M. Li, Q. Wang, G. Wang, Z. Yuan, W. Song, R. Lou, Z. Liu, Y. Huang, Z. Liu, H. Lei *et al.*, Nat. Commun. **12**, 3129 (2021).
[27] Z. Liu, N. Zhao, M. Li, Q. Yin, Q. Wang, Z. Liu, D. Shen, Y. Huang, H. Lei, K. Liu, and S. Wang, Phys. Rev. B **104**, 115122 (2021).
[28] See Supplemental Material at http://link.aps.org/supplemental/10.1103/PhysRevB.105.155108 for details of (i) methods, (ii) magnetism of $\mathrm{XMn_6Sn_6}$ (X = Dy, Tb, and Y), (iii) ARPES measurement orientations, (iv) k_z dispersion of $\mathrm{DyMn_6Sn_6}$, (v) Dirac cone in $\mathrm{XMn_6Sn_6}$, orbital-projected calculation of the band structure of $\mathrm{DyMn_6Sn_6}$, (vi) orbital-projected calculation of the band structure of $\mathrm{DyMn_6Sn_6}$, (vii) calculated band structure of $\mathrm{DyMn_6Sn_6}$ with different onsite Hubbard U of f-electrons, (viii) comparison between the calculated band structures of $\mathrm{XMn_6Sn_6}$, (ix) polarization-dependent measurements of the flat bands, and (x) flat bands measured with circularly polarized photons, which includes Refs. [26,30,31,41–49].

[29] W. Ma, X. Xu, J.-X. Yin, H. Yang, H. Zhou, Z.-J. Cheng, Y. Huang, Z. Qu, F. Wang, M. Z. Hasan, and S. Jia, Phys. Rev. Lett. **126**, 246602 (2021).
[30] B. Malaman, G. Venturini, R. Welter, J. P. Sanchez, P. Vulliet, and E. Ressouche, J. Magn. Magn. Mater. **202**, 519 (1999).
[31] S. Kimura, A. Matsuo, S. Yoshii, K. Kindo, L. Zhang, E. Brück, K. H. J. Buschow, F. R. de Boer, C. Lefèvre, and G. Venturini, J. Alloys Compd. **408–412**, 169 (2006).
[32] N. J. Ghimire, R. L. Dally, L. Poudel, D. C. Jones, D. Michel, N. T. Magar, M. Bleuel, M. A. McGuire, J. S. Jiang, J. F. Mitchell *et al.*, Sci. Adv. **6**, eabe2680 (2020).
[33] F. Ronning, K. M. Shen, N. P. Armitage, A. Damascelli, D. H. Lu, Z. X. Shen, L. L. Miller, and C. Kim, Phys. Rev. B **71**, 094518 (2005).
[34] J. Graf, G. H. Gweon, K. McElroy, S. Y. Zhou, C. Jozwiak, E. Rotenberg, A. Bill, T. Sasagawa, H. Eisaki, S. Uchida, J. Takagi, D. H. Lee, and A. Lanzara, Phys. Rev. Lett. **98**, 067004 (2007).
[35] B. P. Xie, K. Yang, D. W. Shen, J. F. Zhao, H. W. Ou, J. Wei, S. Y. Gu, M. Arita, S. Qiao, H. Namatame, M. Taniguchi, N. Kaneko, H. Eisaki, K. D. Tsuei, C. M. Cheng, I. Vobornik, J. Fujii, G. Rossi, Z. Q. Yang, and D. L. Feng, Phys. Rev. Lett. **98**, 147001 (2007).
[36] T. Valla, T. E. Kidd, W. G. Yin, G. D. Gu, P. D. Johnson, Z. H. Pan, and A. V. Fedorov, Phys. Rev. Lett. **98**, 167003 (2007).
[37] Y. Liu, L. Yu, X. Jia, J. Zhao, H. Weng, Y. Peng, C. Chen, Z. Xie, D. Mou, J. He *et al.*, Sci. Rep. **5**, 13036 (2015).
[38] K. Kim, J. Seo, E. Lee, K. T. Ko, B. S. Kim, B. G. Jang, J. M. Ok, J. Lee, Y. J. Jo, W. Kang *et al.*, Nat. Mater. **17**, 794 (2018).
[39] X. Xu, Y. W. Li, S. R. Duan, S. L. Zhang, Y. J. Chen, L. Kang, A. J. Liang, C. Chen, W. Xia, Y. Xu, P. Malinowski, X. D. Xu, J. H. Chu, G. Li, Y. F. Guo, Z. K. Liu, L. X. Yang, and Y. L. Chen, Phys. Rev. B **101**, 201104(R) (2020).
[40] D. H. Lu, M. Yi, S. K. Mo, A. S. Erickson, J. Analytis, J. H. Chu, D. J. Singh, Z. Hussain, T. H. Geballe, I. R. Fisher *et al.*, Nature (London) **455**, 81 (2008).
[41] Z. Chen, M. Li, C. Liu, Z. Ma, Y. Han, J. Gao, W. Wei, Z. Sheng, and H. Du, Front. Phys. **9**, 685510 (2021).
[42] B. T. Thole, G. van der Laan, J. C. Fuggle, G. A. Sawatzky, R. C. Karnatak, and J. M. Esteva, Phys. Rev. B **32**, 5107 (1985).
[43] P. E. Blöchl, Phys. Rev. B **50**, 17953 (1994).
[44] G. Kresse and D. Joubert, Phys. Rev. B **59**, 1758 (1999).
[45] G. Kresse and J. Hafner, Phys. Rev. B **47**, 558 (1993).
[46] G. Kresse and J. Furthmüller, Comput. Mater. Sci. **6**, 15 (1996).
[47] G. Kresse and J. Furthmüller, Phys. Rev. B **54**, 11169 (1996).
[48] J. P. Perdew, K. Burke, and M. Ernzerhof, Phys. Rev. Lett. **77**, 3865 (1996).
[49] B. C. El Idrissi, G. Venturini, B. Malaman, and D. Fruchart, J. Less Common Metals **175**, 143 (1991).